Weak competing interactions control assembly of strongly bonded TCNQ ionic acceptor molecules on silver surfaces

Changwon Park, Geoffrey A. Rojas, Seokmin Jeon, Simon J. Kelly, Sean C. Smith, Bobby G. Sumpter, Mina Yoon,* and Petro Maksymovych†

Center for Nanophase Materials Sciences, Oak Ridge National Laboratory, Oak Ridge, Tennessee 37831, USA

(Received 31 March 2014; revised manuscript received 18 July 2014; published 19 September 2014)

The energy scales of interactions that control molecular adsorption and assembly on surfaces can vary by several orders of magnitude, yet the importance of each contributing interaction is not apparent *a priori*. Tetracyanoquinodimethane (TCNQ) is an archetypal electron acceptor molecule and it is a key component of organic metals. On metal surfaces, this molecule also acts as an electron acceptor, producing negatively charged adsorbates. It is therefore rather intriguing to observe attractive molecular interactions in this system that were reported previously for copper and silver surfaces. Our experiments compared TCNQ adsorption on noble metal surfaces of Ag(100) and Ag(111). In both cases we found net attractive interactions down to the lowest coverage. However, the morphology of the assemblies was strikingly different, with two-dimensional islands on Ag(100) and one-dimensional chains on Ag(111) surfaces. This observation suggests that the registry effect governed by the molecular interaction with the underlying lattice potential is critical in determining the dimensionality of the molecular assembly. Using first-principles density functional calculations with a van der Waals correction scheme, we revealed that the strengths of major interactions (i.e., lattice potential corrugation, intermolecular attraction, and charge-transfer-induced repulsion) are all similar in energy. The van der Waals interactions, in particular, almost double the strength of attractive interactions, making the intermolecular potential comparable in strength to the diffusion potential and promoting self-assembly. However, it is the anisotropy of local intermolecular interactions that is primarily responsible for the difference in the topology of the molecular islands on Ag(100) and Ag(111) surfaces. We anticipate that the intermolecular potential will become more attractive and dominant over the diffusion potential with increasing molecular size, providing new design strategies for the structure and charge transfer within molecular layers.

DOI: 10.1103/PhysRevB.90.125432 PACS number(s): 68.43.−h, 68.37.Yz, 41.20.Cv, 81.16.Dn

I. INTRODUCTION

The properties of strong electron acceptors and donors on solid surfaces have recently gained more attention in light of the prospects of low-dimensional molecular conductors and charge-transfer compounds [1], control of surface work function in organic electronic devices [2,3], and chemical modification of graphene [4,5] and other two-dimensional (2D) solids. *Tetracyanoquinodimethane* (TCNQ) is the archetypal electron acceptor with large electron affinity of 2.8 eV in the gas phase. Its prominent role in the formation of bulk organic metals, such as Tetrathiafulvalene (TTF)-TCNQ, is well known [6]. Several studies have addressed the properties of surface-supported structures involving TCNQ, where charge transfer likewise must play a prominent role. Alves *et al.* observed metallic conductivity within a single stacked interface of TTF and TCNQ [7]. Studies of TCNQ-based salts on Au(111) surface have shown supermolecular states along the one-dimensional (1D) TCNQ chains dependent on the geometry of neighboring molecules and hybridization with the underlying metal substrate [8]. Most recently weak charge-transfer-induced magnetism was reported for TCNQ adsorbed on graphene [9].

At the same time, any significant charge transfer between the molecule and the substrate or within the molecular layer itself will cause repulsive electrostatic intermolecular interactions. Depending on their strength, formation of ordered structure of adsorbed molecules can be significantly impeded producing disordered or sparse monolayers. The case of TCNQ is quite intriguing in this regard, because of the relatively large amount of charge that can be transferred. According to a recent theoretical analysis with the induced density of interface states (IDIS) model, the extrapolated charge transfer between TCNQ molecules in the monolayer on Ag surface should be 0.2–0.3 e/molecule [10]. For Cu(100) it was reported that 1.5 e can be transferred [11]. Assuming an intermolecular distance of 10 Å and a local charge of 1 e on the molecule, the dipole-dipole repulsion energy between two TCNQ molecules (where the dipole is formed between the molecule and its image charge of separation of 6 Å) is ∼0.5 eV. The intermolecular interactions have similar energy scales making molecular self-assembly marginally possible in this case. At the same time, charge transfer itself may have pronounced coverage dependence due to dipole-dipole repulsion, as in the original depolarization model of Langmuir [12]. In fact, for the TTF molecule—the donor partner of TCNQ in TTF-TCNQ organic metal—it was suggested that the charge transfer can be completely suppressed at monolayer coverage on Au(111) substrate [13].

To investigate these questions further, and to explore the role of the substrate morphology in defining assembly of the TCNQ molecule, we placed TCNQ on the chemically equivalent but geometrically distinct surfaces of Ag(100) and Ag(111). In doing so, we pursued control over periodicity of the underlying lattice potential while retaining largely identical and significant charge transfer. Despite the large binding energy of 2.5–3 eV per molecule, the relatively large size

*myoon@ornl.gov
†maksymovychp@ornl.gov

of TCNQ reduces the corrugation of diffusion potential to the same energy scale as the intermolecular interactions (intermolecular attraction and charge-transfer-induced repulsion), placing all interactions in tight competition with each other. At the same time, the anisotropic shape of the TCNQ molecule translates into a high anisotropy of local potential variation near TCNQ, inducing molecular self-assembly in a preferential direction for a given surface. Consequently, the topology of the molecular layer is dramatically different on both surfaces, being 2D islands on Ag(100) and 1D chains on Ag(111).

II. EXPERIMENTAL SETUP

The experiments were performed using scanning tunneling microscopy (STM) and all samples were grown *in situ* at background pressure of 5×10^{-10} mbar or less. The surfaces of Ag single crystals were prepared by Ar^+ sputtering followed by annealing to 720 K. TCNQ molecules were subsequently deposited on the surfaces by thermal evaporation from a crucible at 370 K onto Ag at 200 K or less. All measurements presented were carried out at 77 K using a Joule-Thomson scanning tunneling microscope (JT-STM, Specs, Berlin) [14]. Tunneling spectra were obtained using constant-current distance-voltage (Z-V) spectroscopy, where the tip displacement is recorded as a function of increasing bias with the feedback maintaining constant current. The change in tip-sample separation (Z-V or its derivative dZ/dV, both with units of nm/V) was used to detect electronic states of the molecules and the surfaces [15,16]. We utilized this methodology, because it allows for spectroscopy at large bias and low tunneling current, minimizing electron-induced molecular reactions. Also, Z-V has a much wider dynamic range compared to I-V spectroscopy for a given gain of the current amplifier.

III. THEORETICAL APPROACHES

We performed total energy calculations to understand the governing interactions of TCNQ molecules on Ag surfaces and their self-assembly mechanism. Our total energy is based on density functional theory (DFT) within the generalized gradient approximation (GGA) for the exchange-correlation functional. The Perdew-Burke-Ernzerhof (PBE) functional form [17] was adopted for the GGA. To capture the long-range dispersion interactions, which are missing in the conventional exchange-correlation functionals, nonempirical van der Waals (vdW) corrections based on the PBE charge densities were performed [18]. Notably, the screening effect in a metallic (Ag) substrate was considered in vdW corrections [19]. Because the atomic polarization of the Ag atom is greatly (about one third) reduced by the collective response of the metallic Ag substrate, this correction is crucial to accurately describe the vdW interaction between a molecule and metal substrate. For example, the TCNQ binding energy of Ag(100) can be overestimated by $\sim$1 eV if the metal screening effects are not incorporated in the vdW interaction. Ionic potentials were described by the projector augmented wave method [20] implemented in the Vienna *Ab Initio* Simulation Package (VASP) [21] and a plane-wave energy cutoff of 400 eV was used for the structural relaxation. For the potential landscape calculation, a TCNQ molecule was translated and fully relaxed until the atomic forces were smaller than 0.02 eV/Å with a constraint that one carbon atom of the central benzene ring is fixed in the lateral direction.

IV. RESULTS AND DISCUSSION

Figure 1(a) shows surface structures composed of both rectangular islands and single molecule chains on the Ag(100) surface at low coverage. The molecules themselves appear as narrow, symmetric features 11 Å $\pm$ 0.5 Å in length and 5.5 Å $\pm$ 0.5 Å in width, each aligned parallel to [110] or [100] lattice vectors. For the ordered arrangements shown, the unit cell dimensions were $\mathbf{a_1} = 12.8$ Å $\pm$ 0.5 Å and $\mathbf{a_2} = 8.5$ Å $\pm$ 0.5 Å enclosing an angle of $\angle \mathbf{a_1 a_2} = 46° \pm 6°$ [Fig. 1(b)]. This corresponds to a parallel offset of $\mathbf{b_1} = 6.9$ Å $\pm$ 0.4 Å and a normal offset of $\mathbf{b_2} = 6.2$ Å $\pm$ 0.4 Å between TCNQ molecules [Fig. 1(b)]. All islands were ordered along one of four axes, rotated in 45° increments relative to one another [Fig. 1(a)]. The one-dimensional chains coalesce after annealing to room temperature while the 2D islands retain a rectangular shape, with length:width ratio between 3:1 and 3:2 along $\mathbf{a_2}$:$\mathbf{a_1}$ [Figs. 1(a) and 1(b)].

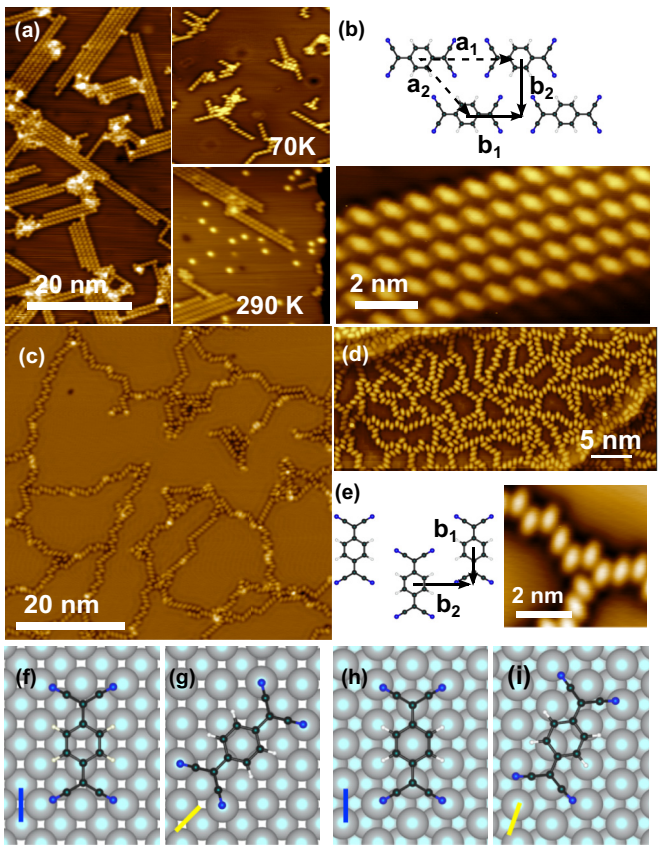

FIG. 1. (Color online) (a) Constant-current STM images of low-coverage TCNQ grown on Ag(100). (b) A schematic of the TCNQ island unit cell and a close-up image of a single TCNQ island. (c) Constant-current STM images of TCNQ following deposition on the Ag(111) at low (c) and higher coverages (d). (e) A schematic of a TCNQ chain on the Ag(111) surface and a close-up STM image of representative chains and junctions between molecules. All images were taken at 77 K. DFT-optimized configurations of TCNQ on Ag(100) (f), (g) and Ag(111) (h), (i).

TCNQ molecules adsorbed on the Ag(111) surface preferentially form 1D chains both at low [Fig. 1(c)] and high TCNQ coverages [Fig. 1(d)]. Individual molecules adsorb in one of two orientations: either almost parallel to the $\langle 1\bar{1}1\rangle$ lattice direction or approximately 30° off axis. The normal offset ($\mathbf{b_2}$) and parallel offset ($\mathbf{b_1}$) between nearest neighbors were 6.5 Å ± 0.2 Å and 3.8 Å ± 0.5 Å, respectively, as shown in the inset of Fig. 1(e). We do not observe linear chain ordering beyond 10 nm within any 2D TCNQ clusters at higher coverage even following thermal annealing to room temperature.

With clean Ag surfaces as a reference, we compared electronic structures of the TCNQ adsorbates using constant-current (Z-V) spectroscopy [Figs. 2(a) and 2(b)] [16]. The energy of the first image potential state (IPS) is ~4.5 eV on Ag(100) [Fig. 2(a)], and 4.5–4.8 V on Ag(111) [Fig. 2(b)]. The energy of IPS obtained from photoemission is approximately 0.6 eV below vacuum energy (E_V) for Ag(111) [22] and 0.5 eV for Ag(100) [23]. Our values are therefore larger than those expected for both surfaces, as the work functions are 4.64 eV [Ag(100)] and 4.75 eV [Ag(111)] [24,25]. The difference is most likely due to Stark shift, to which image potentials are particularly susceptible

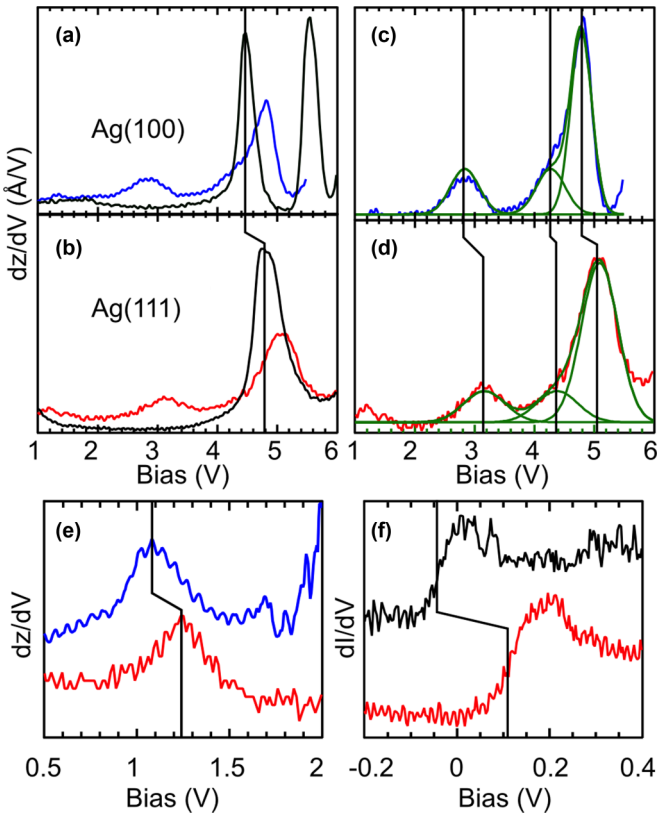

FIG. 2. (Color online) (a) Z-V tunneling spectra of TCNQ/Ag(100) (blue, $I_t = 15$ pA) and of clean Ag(100) surface (black, $I_t = 10$ pA). (b) Z-V spectrum of TCNQ/Ag(111) (red, $I_t = 20$ pA) and of clean Ag(111) (black, $I_t = 8$ pA). (c), (d) Gaussian fits to electronic states on TCNQ/Ag(100) (c) and TCNQ/Ag(111) (d). All spectra shown are averages over at least 20 individual spectra. (f) Energy region around Fermi level probed with dI/dV tunneling spectroscopy. The first harmonic of the modulated signal was recorded with the lock-in amplifier with 5 mV ac modulation at 600 Hz.

[16]. However, if the shifts are similar between tip-surface and tip-molecule-surface junctions, the relative shift of IPS energies provides a direct measure of the change of the work function [15,16]. Z-V spectra of TCNQ/Ag shows very intense features at 4.9 eV for TCNQ/Ag(100) and 5.0 V for TCNQ/Ag(111) [Figs. 2(c) and 2(d)]. We attribute these peaks to blueshifted IPS states, suggesting a roughly equal increase in the surface work function of +0.3–0.5 eV upon adsorption of TCNQ on both systems. This is supported by a measured increase of the barrier height of +0.4 eV ± 0.1 eV on both systems using I-Z spectroscopy [26].

Other peaks observed in the Z-V spectra have energies of 1.1 (1.25) V, 2.9 (3.2) V, and 4.1 (4.25) V in TCNQ/Ag(100) and TCNQ/Ag(111), respectively [Figs. 2(c)–2(e)]. Electronic structures of adsorbed molecules are therefore nearly identical on both surfaces, only shifted by 0.1–0.2 eV relative to each other due to the difference in the work function between original surfaces. The simplest assignment would be to consider these states as lowest unoccupied molecular orbital (LUMO), LUMO+1, and LUMO+2, ignoring the slight degeneracy of the individual molecular states. Indeed, we observe approximately correct, ~1 eV energy difference between LUMO+1 and LUMO+2 states that is very close to that in the gas-phase molecule [27]. From their position relative to E_F, we also surmise a downshift of ~2.5 eV due to combined effects of screening and adsorption. The energy of the lowest-energy peak, however, is too high to be consistent with these values. Electron affinity of gas-phase TCNQ (position of the LUMO) is 2.84 eV below vacuum level [28], which would imply a near overlap with E_F at zero bias. Alternatively, the LUMO-LUMO+1 spacings are incorrect in our case. Without information on the filled states, which was not possible to obtain at this time, we cannot carry out further assignment. No molecular states were observed in the vicinity of the Fermi level, as shown for Ag(111) in Fig. 2(f). The step feature observed in Fig. 2(f) is the surface state of Ag(111), whose energy is upshifted by molecular adsorption similarly to a previous study on Au(111) [29].

In summary, the increase in work function is indicative of substantial charge transfer with TCNQ acting as an electron acceptor [30]. At the same time, the equivalency of electronic structure indicates little difference in the charge transfer between TCNQ on Ag(100) and Ag(111). At the same time, the structures on both surfaces have common asymmetry in adsorbate structure. This is clear in the chainlike TCNQ/Ag(111) structures and the asymmetric length to width ratio in the TCNQ/Ag(100) structures. The latter is indicative of a difference in detachment frequency during the diffusion process and island growth, which suggests anisotropic binding potentials: Those along $\mathbf{b_2}$ are larger than those along $\mathbf{b_1}$ ($E_{\mathbf{b2}} > E_{\mathbf{b1}}$) [31]. This is somewhat similar to the properties of TCNQ/Cu(100), though due to an inherently different process as the asymmetries are opposite with respect to molecular orientation [11].

A quantum mechanical description of systems consisting of even a few TCNQ (each molecule consisting of 20 atoms) molecules on metal substrates (consisting of more than four atomic layers of metals) is highly costly computationally. We therefore simplified the problem by performing a set of calculations for smaller systems to establish a feasible model for the large-scale assembly. First, TCNQ and substrate

interactions were studied by constructing a supercell of a TCNQ molecule on Ag films (thickness of six atomic layers). We constructed a large enough supercell to avoid any artificial interactions between the cells and only Γ-point sampling was performed. Our supercell dimensions were $6a \times 6a \times 40$ Å for TCNQ/Ag(100) and $6a \times 3\sqrt{3}a \times 40$ Å for TCNQ/Ag(111), where a is the lattice constant of fcc Ag of 2.94 Å. We calculated the lattice potential of Ag(100) and Ag(111) [Fig. 3(a)] and the charge transfer from the substrate to the TCNQ upon its adsorption. Second, we accounted for the induced charges on the molecule by a collection of point charges [Fig. 3(c)]. These were assigned to each TCNQ molecule and their electrostatic interactions were calculated. Near the intermolecular distance of 2–8 Å, the electrostatic field of the induced charge transfer can be captured by the dipole field along the z direction and strong local potential in the proximity of nitrogen atoms. The point charges were arranged to reproduce these two conditions. Meanwhile, intermolecular interactions of neutral molecules were investigated without the Ag substrate [Fig. 3(b)]. This estimate included a combination of attractive vdW interactions and hydrogen bonding. This approach greatly reduces the computational cost and we can consider a relatively large molecular assembly for an accurate account of long-range interactions (vdW interaction). Finally, we compiled the complete picture including all relevant interactions extracted from the gas-phase and supercell calculations.

Because TCNQ grows along both $\mathbf{b_1}$ and $\mathbf{b_2}$ directions on Ag(100), the initial orientation of the seed molecule determines the orientation of the 2D assembly. We can infer that the corrugation of the lattice potential plays a significant role in the assembling process of TCNQs from the commensurate orientations with the Ag lattice directions [Figs. 1(f)–1(i)]. Figures 1(f) and 1(h) illustrate the lowest-energy configurations of TCNQ on Ag(100) (binding energy of 2.99 eV) and Ag(111) (binding energy of 2.51 eV), respectively. The local minima configurations displayed in Figs. 1(g) and 1(i) were slightly higher in energy by 0.11 and 0.01 eV, respectively. Starting from the lowest-energy configurations of TCNQ on Ag(100) [Fig. 1(f)] and Ag(111) [Fig. 1(h)], the molecular assembly can grow along either $\mathbf{b_1}$ or $\mathbf{b_2}$ vectors [defined in Fig. 4 for (100) and Fig. 5 for (111)]. We found that at the initial stage of dimer formation, the energy of a dimer along $\mathbf{b_1}$ was higher than that of two separate TCNQs by 0.24 eV, due to the combined effect of electrostatic repulsion and weak intermolecular interaction along $\mathbf{b_1}$. As such, growth along $\mathbf{b_1}$ would be preceded by the growth along $\mathbf{b_2}$, with the assistance of the attractive hydrogen-bonding-like interaction between neighboring molecules [Figs. 4(a) and 5(a)]. This agrees well with our earlier inference of anisotropic binding potential based on the shape of the self-assembled islands.

Figure 4 presents the potential energy profiles of TCNQ on Ag(100) along the trajectories depicted by the vectors $\mathbf{b_1}$ or $\mathbf{b_2}$, where the distance is defined as the displacement from the lattice potential minimum along the $\mathbf{b_1}$ or $\mathbf{b_2}$ directions. Similar calculations were performed for the Ag(111) substrate as shown in Fig. 5. During the growth along $-\mathbf{b_1}$ [Fig. 4(a)], the electrostatic repulsion caused by charge transfer (green) and intermolecular repulsion from Pauli repulsion of the nitrogen electrons (blue) adds to the energy barrier of lattice corrugation (red). As TCNQ approaches its equilibrium position, the intermolecular interaction becomes attractive. The energy gain of −0.36 eV from the intermolecular interaction is mainly contributed by vdW interaction (–0.16 eV) and hydrogen bonding. This attraction overcomes the electrostatic repulsion from charge transfer (∼0.2 eV) and enables 2D assembly. Note that the electrostatic repulsion is anisotropic and effective only when the nitrogen atoms of adjacent molecules are relatively close. From the charge

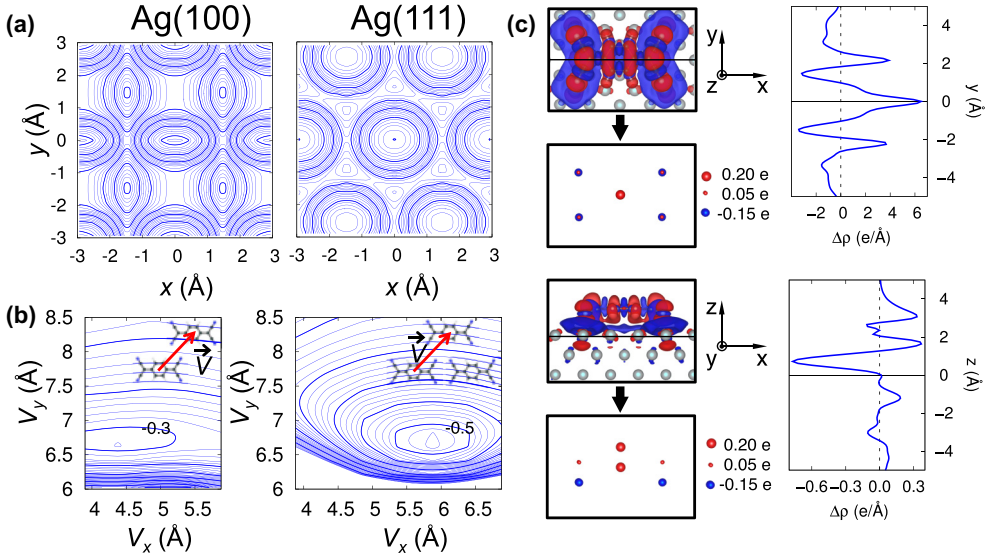

FIG. 3. (Color online) (a) Corrugation of lattice potential of TCNQ molecules on Ag(100) and Ag(111) surface. Thick isolines correspond to 0.1 eV energy spacings. (b) Gas-phase intermolecular interactions are plotted as a function of relative displacement V when they form dimer (left) and trimer (right), where thick isolines correspond to 0.1 eV energy spacings. (c) Difference charge density upon the adsorption of TCNQ on the Ag surface is illustrated by the isosurface of 4.8×10^{-7} $e/\text{Å}^3$ in top and side view, where red represents charge accumulation and blue is for charge depletion. Difference charge density profiles along the y and z axes are shown on the right: $\Delta\rho$ is plane-summed charge along the axes. These charge differences are mapped into the arrays of point charges.

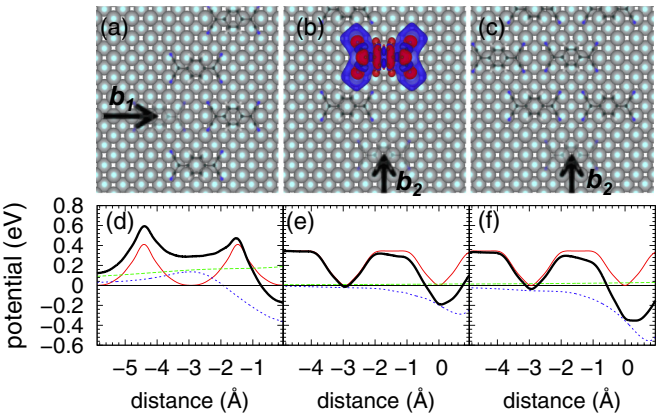

FIG. 4. (Color online) Potential landscapes of a TCNQ molecule introduced into the TCNQ assembly on Ag(100). The displacement directions are indicated by the arrows (a)–(c) and the origin of position is defined by the minimum of lattice potential which lies on the tip of the arrows. The reference of potential energy (i.e., energy zero) is also set to the minimum of lattice potential. (d)–(f) The total potential (black) energy consists of three energy components: lattice potential (red), intermolecular interaction without the substrate (blue), and additional charge-transfer-induced electrostatic intermolecular interaction between negatively charged molecules (green). Difference charge density of TCNQ upon the adsorption on Ag is illustrated by the isosurface of $4.8 \times 10^{-7}\ e/\text{Å}^3$ in (b), where red means a charge accumulation and blue means charge depletion.

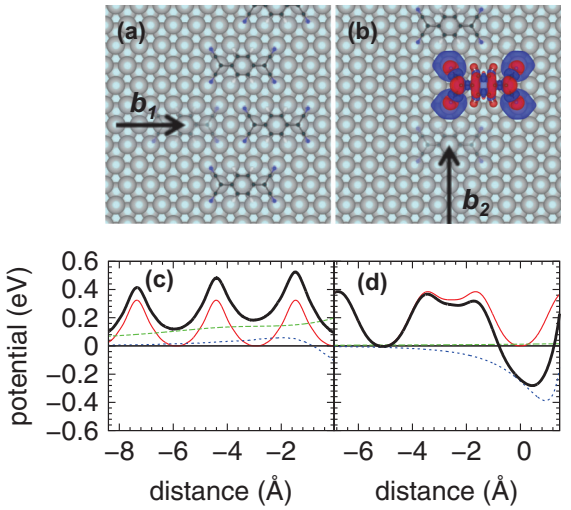

FIG. 5. (Color online) Potential landscapes of a TCNQ molecule introduced into the TCNQ assembly on Ag(111). The displacement directions are indicated by the arrows (a), (b) and the origin of position is defined by the minimum of lattice potential which lies on the tip of the arrows. The reference of potential energy (i.e., energy zero) is also set to the minimum of lattice potential. (c), (d) The total potential (black) energy consists of three energy components: lattice potential (red), intermolecular interaction without the substrate (blue), and additional charge-transfer-induced electrostatic intermolecular interaction between negatively charged molecules (green). Difference charge density of TCNQ upon the adsorption on Ag is illustrated by the isosurface of $4.8 \times 10^{-7}\ e/\text{Å}^3$ in (b), where red means a charge accumulation and blue means charge depletion.

density difference plot of Fig. 3(c), the surface-molecule interaction tends to deplete electrons near the nitrogen atoms and accumulate them on the center of the molecule. Because this quadrupole-type charge distribution decays very fast, adjacent molecules can feel the repulsion only at the proximity of the outermost nitrogen atom. In the case of short axis growth along $-\mathbf{b_2}$, the electrostatic repulsion is much smaller, which lowers the energy barrier. The attractive interaction of 0.2 eV is mainly contributed by intermolecular interaction [Fig. 4(e)].

When 2D assemblies of molecules form (i.e., involving more than pairwise interaction), intermolecular attraction in the gas phase along $\mathbf{b_2}$ is almost doubled [Fig. 4(f)] with respect to the 1D configuration shown in Fig. 4(e). However, the equilibrium position along $\mathbf{b_2}$ becomes considerably offset from the lattice potential minimum and, as such, the structure in Fig. 4(c) might be expected not to be a minimum energy structure. For instance, if we put each molecule on a lattice minimum point along $\mathbf{b_2}$, the intermolecular spacing should be in integer multiplies of the silver lattice constant a (2.94 Å). However, the experimentally observed intermolecular spacing (d) of 6.5 Å ± 0.2 Å for Ag(111) is very close to the minimum distance of intermolecular interaction, d_{min} (∼6.5 Å), which means that a minimum TCNQ structure is incommensurate with the Ag lattice. To further illustrate this, we compare the total energy of a 2D molecular assembly with different spacing (L) along $\mathbf{b_2}$, namely, $L = 3a$, $2.5a$, and $\sim 2.2a$ (d_{min}). The intermolecular spacing $2a$ is excluded because there is a strong repulsion between molecules at such a short distance. Figure 4(f) shows the potential energies of TCNQ as it approaches the 2D assembly, where we can also estimate the energies of different intermolecular spacings d along $\mathbf{b_2}$:

For $L = 3a$ ($d = -1.4$ Å), the intermolecular interaction is very weak and the cohesive energy is almost zero. For $L = 2.5a$ ($d = -0.1$ Å), half of the molecule should sit on the lattice potential maximum of +0.32 eV, but a gain of 0.40 eV from intermolecular attraction reduces the total energy to −0.24 eV, which is energetically more stable than the $L = 3a$ configuration. For $L = d_{\text{min}}$, the attractive intermolecular interaction is maximized to −0.56 eV. In this arrangement, the resulting molecular chain is truly incommensurate with the Ag(100) surface and every lattice point is equally and continuously accessible by molecules; the energy cost is given by the average lattice potential of 0.21 eV shown in Fig. 4(f). By reducing L from $3a$ to $\sim 2.2a$, the net energy gain per molecule (cohesive energy) then becomes 0.35 eV and the total energy is considerably lower by 0.11 eV than that of $L = 2.5a$ structures. In fact, this is reminiscent of the incommensurate solution of the Frenkel-Kontorova model with a strong spring constant (or a weak periodic potential) [32]. We want to stress that this additional large energy gain of 0.11 eV cannot be directly obtained from the affordable size of supercell calculation because of the incommensurable nature of the true ground state. This configuration is classified as the coincidence-1B [33]. The transformation matrix for the epitaxial interface is $\begin{bmatrix} 4 & 0 \\ 2 & \sim 2.2 \end{bmatrix}$, which means that the TCNQ lattice is still commensurate with the Ag lattice along the $\mathbf{b_1}$ direction.

The large difference between the TCNQ assembly on Ag(100) and Ag(111) originates from the relative offset between TCNQs as determined by the underlying lattice.

On Ag(111), the growth process along $\mathbf{b_2}$ is similar to that on Ag(100). The intermolecular attraction then stabilizes the formation of a 1D chain, but growth along $\mathbf{b_1}$ is energetically unfavorable [Fig. 5(c)]. Due to the different underlying lattice geometry, the parallel offset on Ag(111) is smaller than on Ag(100) [Figs. 4(d) and 5(c)] and the attractive interaction between cyano groups and hydrogen atoms of adjacent TCNQ molecules is missing for the TCNQ approaching along $\mathbf{b_1}$ on Ag(111). As a result, the intermolecular attraction along $\mathbf{b_1}$ is considerably lower on Ag(111) than on Ag(100), and it cannot overcome the electrostatic repulsion between negatively charged molecules. Interestingly, it is reported that TCNQ forms 2D assemblies on Au(111) [8]. Because the lattice constant and potential corrugation of gold are very similar to silver, the difference is most likely caused by charge transfer. Due to the negligible charge transfer expected on Au(111), comparatively little electrostatic repulsion relative to TCNQ on Ag(111) would occur. To quantify the assembly process, we consider the potential energy of TCNQ/Ag(111). If the spacing along $\mathbf{b_2}$ is $\frac{\sqrt[3]{3}}{2}a$, which is commensurate to Ag(111), the cohesive energy of a single chain is 0.3 eV [Fig. 5(d)]. The growth along $\mathbf{b_1}$ is unfavorable because of the energy cost induced by the electrostatic repulsion. Contrary to TCNQ/Ag(100), the incommensurate chain of spacing at $d_{\min}$ (6.6 Å) has 0.2 eV (intermolecular minimum 0.4 eV and average lattice potential 0.2 eV) of cohesive energy and it is higher by 0.1 eV than a commensurate chain. The misfit of ∼1 Å between the lattice potential minimum of $\frac{\sqrt[3]{3}}{2}a$ and the intermolecular energy minimum of $d_{\min}$ induces intrinsic intermolecular tension when the molecules are located on exactly commensurate lattice points. Because the intermolecular attraction has a similar strength with the lattice potential, there is a possibility that this tension can be released by concentrating its strain in the form of kinks. Whether kinks form or not depends on the relative strength of intermolecular interaction and lattice potential. In Figs. 1(c) and 1(d), the observed molecular chain in TCNQ/Ag(111) cannot propagate a long distance without changing its orientation and we believe that this is a manifestation of kink structure between two energetically degenerate chains of different orientations.

V. CONCLUSIONS

In summary, by using the chemically equivalent but structurally different surfaces of Ag(111) and Ag(100) we were able to tune the dimensionality of growth for TCNQ charge acceptor systems. The competition between lattice potential, intermolecular attraction, and charge-transfer-induced repulsion determines the tendency toward 1D vs 2D dimensionality on Ag(111) and Ag(100) surfaces. In the meantime, the anisotropic intermolecular potential of the TCNQ translates into anisotropic shapes of molecular assemblies on silver surfaces. The combination of anisotropic molecular shape and lattice potential is quite general for molecular adsorbates, while the corrugation of the lattice potential can be tuned by molecular size. These control handles allow for efficient and deterministic control of molecular assemblies and van der Waals epitaxy.

ACKNOWLEDGMENTS

This work was supported by the Center for Nanophase Materials Sciences, which is sponsored by the Scientific User Facilities Division, office of Basic Energy Sciences, U.S. Department of Energy. M.Y. acknowledges support provided by a Laboratory Directed Research and Development award from Oak Ridge National Laboratory. This research used resources of the National Energy Research Scientific Computing Center, supported by the Office of Science of the U.S. Department of Energy under Contract No. DE-AC02-05CH11231.

[1] D. Jerome, Chem. Rev. **104**, 5565 (2004).
[2] O. T. Hofmann, D. A. Egger, and E. Zojer, Nano Lett. **10**, 4369 (2010).
[3] I. H. Campbell, S. Rubin, T. A. Zawodzinski, J. D. Kress, R. L. Martin, D. L. Smith, N. N. Barashkov, and J. P. Ferraris, Phys. Rev. B **54**, R14321 (1996).
[4] S. Chen, D. C. Qi, X. Y. Gao, and A. Wee, J. Am. Chem. Soc. **129**, 10418 (2007).
[5] S. Y. Zhou, D. A. Siegel, A. V. Fedorov, and A. Lanzara, Phys. Rev. Lett. **101**, 086402 (2008).
[6] G. Saito and Y. Yoshida, in *Unimolecular and Supramolecular Electronics I: Chemistry and Physics Meet at Metal-Molecule Interfaces*, Topics in Current Chemistry Vol. 312, edited by R. M. Metzger (Springer, Berlin, 2012), pp. 67–126.
[7] H. Alves, A. S. Molinari, H. Xie, and A. F. Morpurgo, Nat. Mater. **7**, 574 (2008).
[8] N. Gonzalez-Lakunza, I. Fernández-Torrente, K. J. Franke, N. Lorente, A. Arnau, and J. I. Pascual, Phys. Rev. Lett. **100**, 156805 (2008).
[9] M. Garnica, D. Stradi, S. Barja, F. Calleja, C. Diaz, M. Alcami, N. Martin, A. L. Vazquez de Parga, F. Martin, and R. Miranda, Nat. Phys. **9**, 368 (2013).
[10] J. I. Martínez, E. Abad, F. Flores, and J. Ortega, Phys. Status Solidi B **248**, 2044 (2011).
[11] T.-C. Tseng, C. Urban, Y. Wang, R. Otero, S. L. Tait, M. Alcami, D. Ecija, M. Trelka, J. Maria Gallego, N. Lin, M. Konuma, U. Starke, A. Nefedov, A. Langner, C. Woell, M. Angeles Herranz, F. Martin, N. Martin, K. Kern, and R. Miranda, Nat. Chem. **2**, 374 (2010).
[12] H. S. Taylor, Trans. Faraday Soc. **28**, 131 (1932).
[13] J. Fraxedas, S. Garcia-Gil, S. Monturet, N. Lorente, I. Fernandez-Torrente, K. J. Franke, J. I. Pascual, A. Vollmer, R. P. Blum, N. Koch, and P. Ordejon, J. Phys. Chem. C **115**, 18640 (2011).
[14] G. A. Rojas, P. Ganesh, S. J. Kelly, B. G. Sumpter, J. A. Schlueter, and P. Maksymovych, J. Phys. Chem. C **117**, 19402 (2013).
[15] D. B. Dougherty, P. Maksymovych, J. Lee, and J. T. J. Yates, Jr., Phys. Rev. Lett. **97**, 236806 (2006).
[16] D. B. Dougherty, P. Maksymovych, J. Lee, M. Feng, H. Petek, and J. T. J. Yates, Jr., Phys. Rev. B **76**, 125428 (2007).
[17] J. P. Perdew, K. Burke, and M. Ernzerhof, Phys. Rev. Lett. **77**, 3865 (1996).

[18] A. Tkatchenko and M. Scheffler, Phys. Rev. Lett. **102**, 073005 (2009).
[19] V. G. Ruiz, W. Liu, E. Zojer, M. Scheffler, and A. Tkatchenko, Phys. Rev. Lett. **108**, 146103 (2012).
[20] G. Kresse and D. Joubert, Phys. Rev. B **59**, 1758 (1999).
[21] G. Kresse and J. Furthmuller, Phys. Rev. B **54**, 11169 (1996).
[22] W. R. Merry, R. E. Jordan, D. F. Padowitz, and C. B. Harris, Surf. Sci. **295**, 393 (1993)
[23] K. Giesen, F. Hage, F. J. Himpsel, H. J. Riess, and W. Steinmann, Phys. Rev. B **35**, 971 (1987).
[24] B. Reihl, K. H. Frank, and R. R. Schlittler, Phys. Rev. B **30**, 7328 (1984).
[25] D. Straub and F. J. Himpsel, Phys. Rev. B **33**, 2256 (1986).
[26] G. Binnig, N. Garcia, H. Rohrer, J. M. Soler, and F. Flores, Phys. Rev. B **30**, 4816 (1984).
[27] J. Fraxedas, Y. J. Lee, I. Jiménez, R. Gago, R. M. Nieminen, P. Ordejón, and E. Canadell, Phys. Rev. B **68**, 195115 (2003).
[28] R. N. Compton and C. D. Cooper, J. Chem. Phys. **66**, 4325 (1977).
[29] I. F. Torrente, K. J. Franke, and J. I. Pascual, Int. J. Mass Spectrom. **277**, 269 (2008).
[30] N. Koch, S. Duhm, J. P. Rabe, A. Vollmer, and R. L. Johnson, Phys. Rev. Lett. **95**, 237601 (2005).
[31] A. Kuehnle, Curr. Opin. Colloid Interface Sci. **14**, 157 (2009).
[32] M. Peyrard and S. Aubry, J. Phys. C: Solid State Phys. **16**, 1593 (1983).
[33] D. E. Hooks, T. Fritz, and M. D. Ward, Adv. Mater. **13**, 227 (2001).